Evaluating Variations in Great Salt Lake Inflow to Infer Human Consumptive Water Use, A Volume Reconstruction Approach

M. F. Merck[1] and D. G. Tarboton[1]

[1] Utah Water Research Laboratory, Utah State University, Logan, Utah, USA

Corresponding author: Madeline Merck (madelinemerck@yahoo.com)

Key Points:

- Current estimates of consumptive water use that apply direct calculation methods for the Great Salt Lake Basin are disparate
- Flow reductions into the lake due to consumptive use can be estimated using volume reconstruction and lake level measurements
- Our volume reconstruction consumptive use estimate of 2.3 km^3/yr independently corroborates direct calculations

Abstract

The declining water level in Great Salt Lake (GSL) has been attributed to human consumptive water use that depletes natural streamflow into the lake. Understanding depletions due to historical consumptive water use within the GSL Basin is important to managing present and future lake conditions. Direct calculations of consumptive water use in the basin are made by summing detailed uses and return flows. However, this method is limited by insufficient data and resulting estimates thus far have been disparate. In this study, we reconstructed total GSL water inputs and stream inflows using lake levels recorded from 1847-2023 to estimate the magnitude of reductions due to consumptive use and the associated lake level decline. To do so, we developed a method that uses lake volume changes derived from bathymetry and water surface elevation measurements along with estimates of annual evaporation and precipitation over the lake to hindcast inflow volume to the lake. The declining trend in lake inflow, without associated precipitation or natural streamflow trends, was used to quantify basin wide water depletions to be up to 2.3 km^3/yr and the current lake level decline associated with this estimate to be as much as 4.6 meters. This basin wide depletion estimate depends only on lake level, precipitation, and evaporation estimates and is not limited by the challenges of aggregating individual diversions and return flows.

Plain Language Summary

The Great Salt Lake (GSL) is an ecologically and economically important resource that is at risk due to declining lake levels. This decline has been attributed to human consumptive water use that depletes streamflow into the lake. Understanding depletions due to consumptive water use within the GSL Basin is important to managing present and future lake conditions. We reconstructed total GSL water inputs using lake levels recorded from 1847-2023. Calculations of lake volume changes associated with measured lake level changes, together with information on direct precipitation to and evaporation from the lake, support the estimation of lake inflow back to the date lake levels were first recorded and prior to the dates for which streamflow has been measured. Trends associated with these prior streamflow hindcasts were used to infer overall consumptive use depletion of streamflow and the impact this has had on lake levels. This approach complements and extends direct approaches for calculating consumptive use depletion of streamflow in the GSL Basin. The results are important because they quantify how consumptive use has impacted the lake and serve as a reference for efforts towards conservation and other water management actions aimed at restoring the lake to more healthy levels.

1 Introduction

The Great Salt Lake (GSL) is a terminal lake located in northern Utah within the Great Basin (Figure 1). It is the largest terminal lake in North America. The lake is divided into two arms by a railroad causeway that was built in 1959. The south arm, Gilbert Bay, receives

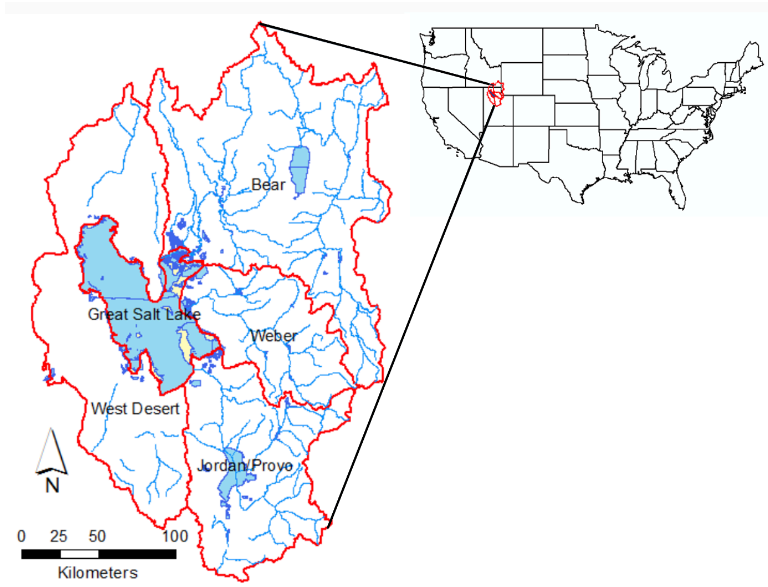

Figure 1. Location of the Great Salt Lake and its contributing basins.

approximately 95% of the surface inflow to the lake entering along the southeastern shores from three major rivers, Bear, Weber, and Jordan (Loving et al., 2000). In the north arm, Gunnison Bay, input is limited to direct precipitation and intermittent runoff. Gilbert Bay is roughly twice the area and volume of Gunnison Bay. Evaporation is the only outflow from either arm, resulting in the lake's high salinity (e.g., Loving et al., 2000). Level, area, and volume of GSL adjust to balance differences in these inflows and outflows and, with its large size and relatively shallow depth (13 meters at its deepest), area and volume vary greatly with fluctuating levels.

In recent years, the GSL water surface elevation (WSE) has declined to critically low levels, with much of the decline being attributed to depletion of streamflow through human consumptive water use (Wurtsbaugh et al., 2017). This is superimposed on natural climate driven low frequency cycles and periodic extremes (Lall and Mann, 1995). There is thus a need to quantify historical reductions in inflow to the GSL due to the depletion of streamflow and associated declines of GSL WSE. However, while GSL WSE has been measured since 1847, streamflow measurements from all the main lake inflows are complete only following 1949. Much development of agricultural water use within the GSL Basin started immediately upon settlement of the GSL valley by European (Mormon) settlers in 1847. The impacts of the resultant reductions in streamflow are therefore already part of streamflow measurements making it difficult to determine reductions in streamflow due to water use depletions from current trends in streamflow measurements alone.

Mohammed and Tarboton (2012) defined a GSL volume sensitivity measure, denoted as ϕ, as the ratio of the standard deviation of input variables to the standard deviation of the lake volume change at an annual time scale. They found that lake volume is eight times more sensitive to streamflow ($\phi = 0.83$) than evaporation ($\phi = 0.10$) and nearly three times more sensitive than precipitation ($\phi = 0.30$). The strong relationship between lake volume changes and streamflow suggests that volume changes derived from changes in WSE may be useful to infer inflow to GSL back to the time when levels were first measured and thus extract information not available in post 1949 streamflow measurements on how streamflow may have been reduced by water use development.

Tree-ring reconstructions of streamflow extend several centuries into the past and provide information on streamflow prior to the availability of measurements. Based on climate and soil moisture driven growth of trees, tree ring reconstructions are not impacted by diversions and thus represent estimates of natural flow. Streamflow reconstructions from tree-ring estimates dating back approximately 1200 years for the Bear River (DeRose et al., 2015), 600 years for the Weber River (Bekker et al., 2014), and 800 years for the Jordan River (Tikalsky, 2007) show no significant long-term trends. Therefore, any trend in streamflow into the lake inferred from lake volume changes over the period of human development prior to the availability of complete lake inflow streamflow measurements can be attributed to human influence reflecting streamflow depletion due to consumptive use (CU).

The goal of this paper was to investigate and reconstruct streamflow into GSL from volume change measurements and, from trends in these reconstructions, infer how human consumptive water use has impacted streamflow. Our approach is an alternative to, and check or validation of, uncertain and unknown early direct consumptive use depletion estimates. We developed a volume reconstruction approach to reconstruct the historical record of annual inflow to GSL for U.S. water years 1848-2023 by using lake volume changes along with evaporation and precipitation hindcasts as inputs to a water mass balance for the lake. Our hindcast and mass balance process, along with supporting assumptions, are described in the methods section. The objective was to establish the magnitude of streamflow reductions due to CU based on mass balance evidence in the historical record for GSL WSE as an alternative to and check on direct CU streamflow depletions that are only available during recent periods and are uncertain. Trends from the reconstructed inflow were used to estimate CU in the GSL Basin and how, over the period that WSE has been measured, CU as led to changes in WSE.

2 Background

Both arms of GSL have a salt concentration several times higher than the ocean. The hypersaline lake and associated marshes are vital for breeding and migrating shorebirds (IWJV, 2016). The Western Hemisphere Shorebird Reserve Network has designated the GSL as a site of Hemispheric Importance, the highest rank of importance (WHSRN, 2016). A major food source for the birds is the lake’s brine shrimp, which are also considered a keystone species because they control the lake’s phytoplankton (Stephens, 1990; Aldrich and Paul, 2002). Brine shrimp harvesting is also important economically. GSL is the largest source of brine shrimp for the global aquaculture industry, feeding an estimated 10 million metric tons of farmed seafood each year (Penrod, 2023; Brown et al., 2023). The north arm of GSL can no longer support brine shrimp or brine fly populations due to extremely high salinities (Barnes & Wurtsbaugh, 2015). Although the less saline south arm does not support fish, brine shrimp and brine flies flourish in most years (WHSRN, 2016). However, salinity nearing or reaching biotic thresholds can be harmful to the brine shrimp and brine flies. Disruptions in the brine shrimp and brine fly population propagate and result in disturbances further up the food chain, affecting migratory bird populations and food production for human consumption.

The south arm is also home to the estuaries of Bear River Bay and Farmington Bay. Both bays receive freshwater inflows and, therefore, have lower salinity than the rest of the lake. When GSL WSE is at or above what is regarded as normal elevations (average ~4200 feet or

1280 meters), these bays provide shorebird habitat and are commonly used for recreation. However, being shallower areas of the lake, both bays are nearly dry at current low lake levels and the possibility of complete desiccation is a real threat. In addition, the ecosystems in these bays are fragile and struggle under low WSE conditions (Wurtsbaugh et al., 2016).

Low WSE and high salinities throughout the lake also make it more difficult to pump lake water to the evaporation ponds for mineral extraction, which are located on the periphery of the lake. In 2014, Morton Salt dug a five-mile-long canal in the south arm to deliver brine from the distant lake water to their salt ponds and processing plants (Wurtsbaugh et al., 2016). US Magnesium (MagCorp), a producer of magnesium located on the south arm, is also extending their canals by several miles (UDEQ, 2022). In the north arm, accumulating salt precipitate as thick as 8 feet requires repeated dredging from the Behrens Trench, an underwater canal used in the mineral extraction process by Compass Minerals (Standard Examiner, 2016; FGSL, 2018).

Another problem created by low WSE is increased lakebed exposure, which increases the potential for dust pollution and related human health impacts due to dust from the exposed shores (Hahnenberger and Nicoll, 2012; 2014). This is worrisome due to the proximity to Salt Lake City and its growing metropolitan area. Recent work has also attributed significant dust from exposed GSL lakebed area with earlier snowmelt due to dust on snow albedo reductions (Lang et al., 2023). All of the concerns mentioned here that threaten the lake's uses are exacerbated by low WSE. Therefore, water use in the GSL Basin and its effect on the lake are important to understand and manage.

Following the settlement of Salt Lake City in 1847 by Mormon pioneers, the population of Utah has grown steadily (Figure 2a). Much of this growth is centered around Salt Lake City and is within the basins draining into GSL. With increased population comes increased demands on the land and its resources, including water. Agricultural irrigation is the largest water consumer in Utah, accounting for over 70% of the state's water use (UGS, 2021), with other uses making up the balance (Figure 2b). Increases in water use within the GSL Basin impact WSE, volume, and salinity and, therefore, the many uses of the lake.

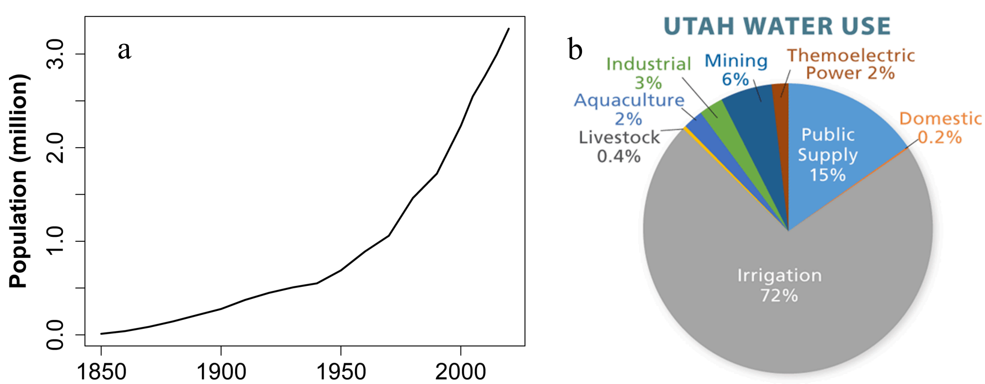

Figure 2. a) Population of Utah, 1850-2020. b) Water use in Utah (UGS, 2021).

In recent years, there have been efforts to estimate CU for the GSL Basin. However, existing estimates of CU in the literature are disparate. For example, Wurtsbaugh et al. (2017) estimate present day total annual CU to be ~1.7 km^3 while the GSL Strike Team (GSLST, 2023) estimate is ~2.6 km^3 (Figure 3), more than a 50% difference. The GSL Strike Team reported individual year CU for the contemporary period, 1989-2020, and found CU within that period to

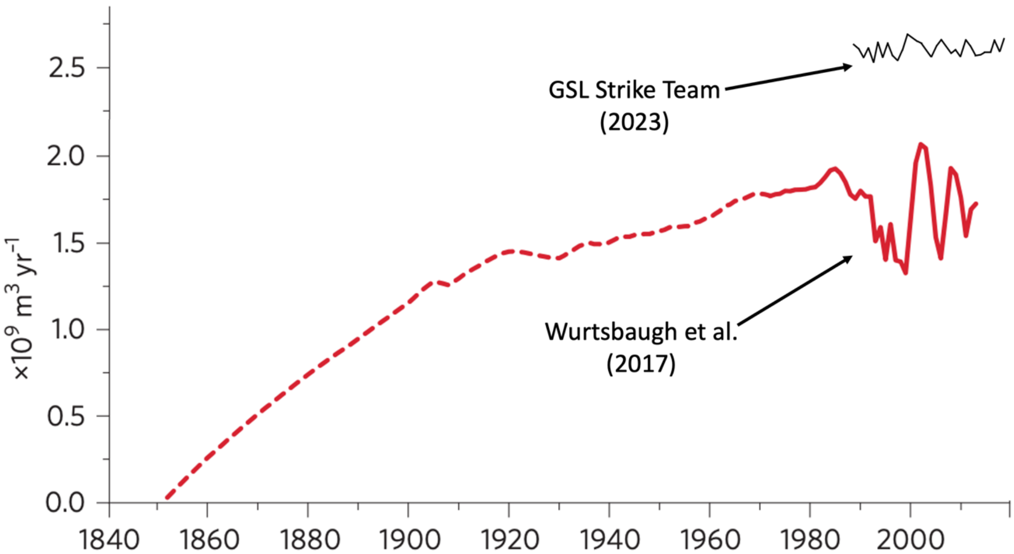

Figure 3. Contrasting estimates of consumptive use for the GSL Basin, including historical consumptive water use from Wurtsbaugh et al (2017, red line), and contemporary consumptive use reported by GSL Strike Team (2023, black line). Consumptive uses prior to 1989 (dashed line) are estimated and based on unpublished data from Utah Division of Water Resources (Wurtsbaugh et al., 2017).

be fairly consistent with no overall trend (black line, Figure 3). Wurtsbaugh et al. infers CU back to ~1850 and their estimate (red line, Figure 3) suggests that the majority of CU growth occurred shortly after the GSL Basin was settled, prior to the turn of the century and prior to complete stream gaging (red dashed line, Figure 3). Wurtsbaugh et al. (2017) also estimated that the total CU in the GSL Basin between ~1850 and present day has decreased the WSE of GSL by over 3 meters. These direct approaches to quantifying CU are challenging as they involve the aggregation of uncertain inputs, including summaries of land use and estimates of evapotranspiration, ungauged inflows, and irrigation return flows (Wurtsbaugh et al., 2017). This disparity is a motivating factor for this study to estimate and corroborate water use independently through a whole basin water balance approach based on the recorded history of lake levels.

3 Methods

The water mass balance equation for a closed basin lake such as GSL may be stated as:

$$Change\ in\ Volume\ =\ Inflow\ +\ Precipitation\ -\ Evaporation \qquad (1)$$

Or equivalently, given our interest in estimating streamflow prior to its measurement, as:

$$Inflow\ =\ Change\ in\ Volume - Precipitation\ +\ Evaporation \qquad (2)$$

This offers opportunities for estimating hindcast Inflow through measurements of the change in volume and estimates of lake precipitation and evaporation. Change in Volume can be calculated from WSE data, which are available starting in 1847 through the USGS National Water Information System website (USGS Site Numbers 10010000 and 10010100, in https://maps.waterdata.usgs.gov/mapper, accessed on 1 November 2023). Precipitation data over the GSL Basin are available to a varying degree of quality from sources such as PRISM since approximately 1900 (Daly et al., 2008, https://prism.nacse.org). Evaporation has not been directly measured and is generally calculated from mass balance closure, which limits its availability to 1949 to present due to the availability of streamflow data. Therefore, to extend estimates of Inflow back over times prior to its measurement, suitable assumptions or approximations must be made for Precipitation and Evaporation.

Here we evaluated a total of four approaches to hindcasting annual inflow to GSL for U.S. water years 1848-2023. Note that in the U.S. a water year is defined to run from October 1 of the previous year to September 30 of the designated year. Year in this paper always refers to water year unless noted otherwise. For all four approaches, we assumed that the depth of freshwater equivalent lake evaporation each year was constant at its average value. The first three approaches use different assumptions for approximating precipitation. First, because precipitation data is not available for the full duration of our study, we assumed precipitation depth was constant at its long-term average value. Second, recognizing that precipitation and streamflow are correlated, we assumed a constant runoff ratio and constant proportion between basin and lake precipitation. Third, we hindcast streamflow using PRISM precipitation data for the period they are available. For the fourth hindcast approach, we included precipitation volume with the inflow quantity being hindcast, effectively estimating streamflow plus precipitation from volume changes as the hindcast quantity. This approach avoids introducing uncertainty due to not knowing precipitation, and instead transfers the uncertainty to the interpretation of the combined input quantity hindcast. These four approaches all exploit the fact, reported by Mohammed and Tarboton (2012), that GSL Change in Volume is significantly more sensitive to Streamflow variability than Precipitation or Evaporation variability and, therefore, that the sensitivity of hindcast Inflow to errors introduced through approximating Precipitation and Evaporation is likely to be relatively small. The uncertainty in these inflow hindcasts was quantified through comparison of their estimates to actual streamflow and, in the case of the runoff ratio based precipitation hindcast, to PRISM precipitation over the periods when there is streamflow and precipitation data. Common hydrologic performance metrics (Nash-Sutcliffe Efficiency, Kling-Gupta Efficiency, Root Mean Square Error) were used to quantify this uncertainty. These hindcasts were then used to infer how lake inputs (either streamflow or streamflow plus precipitation) have reduced since lake levels were first measured, presumably due to the development of water resources and CU. In each of the subsections below, we give details of the calculations and equations involved.

3.1 GSL Specific Water Mass Balance

To fully describe the process of developing a hindcast estimate of the Inflow specific to streamflow into GSL, a more detailed expression of Equation 1 is shown in Equation 3.

$$\Delta V = V_i(WSE_i) - V_{i-1}(WSE_{i-1}) = Q_S + Q_G + Q_{ME} + Q_{WD} + P_L * A_L - E_L * A_L \qquad (3)$$

As expressed here, ΔV = Change in Volume; Inflow has been separated into Q_S = surface inflow (streamflow) volume, Q_G = groundwater flow volume, Q_{ME} = mineral extraction pumping (negative) and return flow volume (positive), and Q_{WD} = west desert pumping (negative) and return flow volume (positive); Precipitation has been expressed as P_L = precipitation depth over the lake times A_L = area of the lake; and Evaporation as E_L = evaporation depth over the lake times A_L. Lake volume and lake area are both functions of WSE through the bathymetry of the lake; WSE is the quantity that has been measured over time. Equation 3 can be reformulated to solve for surface inflow volume, Q_S.

$$Q_S = \Delta V - Q_G - Q_{ME} - Q_{WD} - P_L * A_L + E_L * A_L \quad (4)$$

This formulation can be used to estimate the hindcast of historical inflow to GSL once data, assumptions, and approximations for variables on the right-hand side are established. In this formulation, ΔV and A_L are calculated directly from WSE measurements back to 1847. Constant Groundwater Inflow, Q_G, is estimated based on prior work (Waddell and Fields, 1977). Mineral extraction, Q_{ME}, and west desert pumping, Q_{WD}, are known quantities and are 0 prior to when they began in 1960 and 1987, respectively. This leaves the variables P_L and E_L to be estimated in order to use Equation 4 for hindcasting. Flow quantities and lake areas were evaluated using annual or 12-month average data for the U.S. water year starting October 1. Lake volumes were taken as end of water year values so that ΔV was a water year difference associated with the period over which the flows were averaged.

3.2 Inflow

In Equation 4, inflow to GSL is separated into streamflow volume (Q_S), groundwater flow volume (Q_G), mineral extraction pumping and return flow volume (Q_{ME}), and west desert pumping and return flow volume (Q_{WD}). We used streamflow data from the United States Geological Survey (USGS), https://maps.waterdata.usgs.gov/mapper/ (accessed 1 June 2023). Missing data was filled in using regression with nearby stations to create a complete $Q_{S,measured}$ dataset for 1950-2023 using methods documented by Tarboton (2023) that were adapted from Loving et al. (2000) and Mohammed and Tarboton (2012). Waddell and Fields (1977) estimated annual GSL groundwater inflow to be $Q_G = 0.0925$ km^3/year. We took this quantity as a constant for the entire 1848-2023 period due to the lack of information on temporal variability of groundwater inflows. There is uncertainty in this assumption, but errors due to this assumption are expected to be small due to the small overall contribution from groundwater. The West Desert Pumping Project circulated water out of GSL from 1987-1989 and then back to GSL from 1990-1992. Flow estimates for Q_{WD} were obtained from Loving et al. (2000). Mineral extraction in GSL started in the 1960s. Flow rates for Q_{ME} were estimated based on withdrawals reported by mineral industries to the Utah Division of Water Rights. More detailed information can be found on the Q_{WD} and Q_{ME} time series in Merck and Tarboton (2023).

3.3 Area and Volume

Lake area and lake volume are functions of WSE. They were tabulated in 0.15 m (0.5 foot) increments, for elevations from 1269.5 m to 1286.45 m, from the lakebed bathymetry digital elevation model (Tarboton and Merck, 2023) using methods detailed in Merck and Tarboton (2023). The historical time series of WSE was used to interpolate time series of A_L, V, and hence ΔV needed for our analysis from the lake area and volume bathymetry tables. This paper used the total volume in each arm of the lake, including areas now separated into mineral extraction evaporation ponds because, at the times the lake was high, these pond areas were effectively part of the lake due to either being breached or not yet being constructed and our focus is on inferring what inflows were prior to pond construction.

3.4 Evaporation

Measured evaporation data is not available for GSL. However, all other terms in Equation 3 are available from 1949 to present. Thus, Equation 3 can be rearranged to calculate evaporation for the years 1950-2023 using mass balance closure.

$$E_{L,MB} = \frac{Q_S + Q_G + Q_{ME} + Q_{WD} + P_L * A_L - \Delta V}{A_L} \quad (5)$$

Recognizing that evaporation is sensitive to salinity, which changes from year to year, the evaporation term is further expressed as

$$E_{L,MB} = E_{f,MB} * SCF \quad (6)$$

where $E_{f,MB}$ = mass balance freshwater evaporation and SCF = salinity correction factor, which reduces freshwater evaporation based on salinity. The freshwater evaporation depth over the lake, $E_{f,MB}$, can be calculated for 1950-2023 using Equation 6 once the SCF has been calculated. Mohammed and Tarboton (2012) developed a modification to the Penman method for calculating lake evaporation based on salinity using an activity coefficient to reduce saturation vapor pressure. This was used to calculate GSL evaporation over the period of their study. Comparing their salinity dependent evaporation and freshwater evaporation, we developed the following empirical equation for SCF as a function of salinity, S.

$$SCF = -1 \times 10^{-11} * S^4 + 3 \times 10^{-9} * S^3 - 2 \times 10^{-4} * S + 1 \quad (7)$$

Salinity is required to use Equation 7 and was calculated based on salt mass divided by lake volume, $S = M_{salt}/V_{Lake}$, where V_{Lake} is a function of bathymetry and WSE. Merck and Tarboton (2023) estimated GSL salt mass based on salinity and volume measurements for the period 1966 to present. Salt mass prior to 1966 was inferred based on the salinity of river inputs (Hahl, 1968). The mean $E_{f,MB}$ for 1950-2023, $E_{f,mean}$, was used along with estimated SCF to calculate the times series of evaporation depth over the lake, E_L, for 1848-2023.

$$E_L = E_{f,mean} * SCF \quad (8)$$

3.5 Precipitation

Gridded data for precipitation depth are available with a 4 km resolution for the years 1895 to present from the PRISM Climate Group based at Oregon State University (https://prism.nacse.org, accessed 1 June 2023). PRISM uses interpolation based on physiographic similarity to estimate precipitation from discontinuous and intermittent point observations (Daly et al., 2008). PRISM estimates do suffer from uncertainty, especially during the early years, when the underlying point observations are sparse. There are also other gridded precipitation data sources (e.g., NLDAS, DAYMET, gridMET) available in easy-to-use format from sites such as climateengine.org (Huntington et al., 2017), but these start no earlier than 1950. We performed spot check comparisons of PRISM precipitation versus some of these other sources, and versus point observations for some long running precipitation stations in the GSL basin, and found differences to be generally small, though there were some sites with notable biases. We decided that relying on the specialized functionality built into PRISM methods for interpolation and addressing shortcomings due to missing data was preferable to us attempting our own interpolation from point precipitation observations. Thus, our analysis has used PRISM data.

PRISM precipitation data were extracted for the area of the three river basins (Bear, Weber and Jordan) that contribute to streamflow into GSL, $P_{B,PRISM}$, and the area over the lake, $P_{L,PRISM}$, for the full duration of the PRISM dataset. A hindcast of precipitation was still needed for 1848-1895, the years for which PRISM is not available, and, as noted above, we evaluated two options: (1) constant precipitation at its long-term average value; and (2) lake precipitation estimated from runoff ratio and the ratio with basin precipitation being assumed constant.

Detailing the second approach, streamflow volume in a basin is related to the precipitation volume over that basin through the runoff ratio, r, expressed as

$$r = \frac{Q_S}{P_B * A_B} \tag{9}$$

where Q_S = streamflow volume in the basin, P_B = precipitation depth over the basin, and A_B = 35,637 km^2, the area of the combined Bear, Weber, and Jordan River basins. While r varies year to year, an average value for r was estimated based on years 1950-2023, the time span data is available for all three variables in Equation 9. Another assumption is that the precipitation depth over the basin and the precipitation depth over the lake are linearly related

$$P_B = a * P_L \tag{10}$$

where a = basin to lake precipitation ratio and P_L = precipitation depth over the lake. A value for a was estimated based on PRISM data, $P_{B,PRISM}$ and $P_{I,PRISM}$, for the years 1896-2023. Average values for r and a were substituted into Equation 3 and then solved for precipitation depth over the lake

$$P_{L,ra} = \frac{\Delta V - Q_G - Q_{ME} - Q_{WD} + E_{f,mean} * SCF * A_L}{(r * a * A_B + A_L)} \tag{11}$$

All variables on the right side of Equation 11 now have either measured data or have been estimated for the years 1848-2023 and can be used to estimate a time series of precipitation depth over the lake, $P_{L,ra}$.

3.6 GSL Inflow Hindcasts

To supplement the USGS measured streamflow record, $Q_{S,measured}$, Equation 4 was used to estimate two hindcast time series for inflow to GSL for the full period of record, 1848-2023, using the two different assumptions about precipitation over the lake, and another inflow hindcast was estimated using PRISM precipitation data for 1896-2023, the years PRISM data is available. Note that both Q_{WD} and Q_{ME} are zero for years 1848-1949, the time period over which the hindcasts of inflow to GSL will be used to supplement measured data, but both variables have been retained in the equations that follow for the purpose of validating hindcast estimates for the years 1950-2023.

The first hindcast inflow to GSL, $Q_{S,Pmean}$ or just the *Pmean* hindcast, was calculated for 1848-2023 using Equation 4 based on the assumption of constant depths for precipitation and freshwater evaporation over the lake. The mean of the PRISM time series data for the years 1896-2023, $P_{L,mean}$, was used for precipitation depth, P_L. The mean of the mass balance freshwater evaporation depth for the years 1950-2023, $E_{f,mean}$, was used for freshwater evaporation depth, E_f, along with estimated SCF for the years 1848-2023. Substituting these variables into Equation 4 we get

$$Q_{S,Pmean} = \Delta V - Q_G - Q_{ME} - Q_{WD} - P_{L,mean} * A_L + E_{f,mean} * SCF * A_L \tag{12}$$

The second hindcast inflow to GSL, $Q_{S,ra}$ or just the *ra* hindcast, was also calculated for 1848-2023 using constant freshwater evaporation depth over the lake in Equation 4. However, this hindcast used the assumption that the runoff coefficient, r, and precipitation ratio, a, are both constant over the years 1848-2023, and therefore the hindcast precipitation, $P_{L,ra}$, was used for precipitation, P_L. Substituting into Equation 4 we get

$$Q_{S,ra} = \Delta V - Q_G - Q_{ME} - Q_{WD} - P_{L,ra} * A_L + E_{f,mean} * SCF * A_L \tag{13}$$

A third hindcast inflow to GSL, $Q_{S,PRISM}$ or just the *PRISM* hindcast, was calculated using PRISM data, $P_{L,PRISM}$, and constant freshwater evaporation depth over the lake in Equation 4 for the dates PRISM data is available, 1896-2023. Substituting into Equation 4 we get

$$Q_{S,PRISM} = \Delta V - Q_G - Q_{ME} - Q_{WD} - P_{L,PRISM} * A_L + E_{f,mean} * SCF * A_L \tag{14}$$

The PRISM hindcast was used in both reconstructions of inflow to GSL for the years 1896-1949, the years PRISM data are available but streamflow data is not.

3.7 Primary Inputs Hindcast: $Q + P$ Using ΔV and Constant E_L

Equation 3 can be rearranged to calculate the primary inputs to GSL, inflow and precipitation, using mass balance closure as follows

$$Q_S + P_L * A_L = \Delta V + E_L * A_L - Q_G - Q_{ME} - Q_{WD} \tag{15}$$

All variables on the right-hand side of Equation 15 are known or have reasonable approximations for the years 1848-2023. This fourth hindcast provides information on the total input to the lake without the uncertainties introduced by precipitation assumptions and serves as another line of evidence quantifying reduced inputs.

3.8 GSL Inflow Reconstructions

Inflows to GSL were reconstructed using inflow hindcasts and measured streamflow. The *Pmean* and *ra* hindcasts were used for 1848-1895, the years there is no precipitation, evaporation, or streamflow data available. The *PRISM* hindcast was used for 1896-1949, the years there is PRISM precipitation data available but no evaporation or streamflow available. And measured streamflow was used for 1950-2023.

$$\begin{aligned} Q_{R,Pmean} = concatinate(&Q_{S,Pmean}(1848-1895), \\ &Q_{S,PRISM}(1896-1949), Q_{measured}(1950-2023)) \end{aligned} \tag{16}$$

$$\begin{aligned} Q_{R,ra} = concatinate(&Q_{S,ra}(1848-1895), \\ &Q_{S,PRISM}(1896-1949), Q_{measured}(1950-2023)) \end{aligned} \tag{17}$$

These inflow reconstructions were used to determine the associated input reductions, natural flow, and WSE for GSL.

3.9 Consumptive Use and Natural Flow

The natural flow of a stream, Q_N, is equal to the measured streamflow, Q_S, plus the reductions due to water depletions for its basin, Q_D.

$$Q_N = Q_S + Q_D \tag{18}$$

Historical streamflow in the GSL Basin measured at points above diversions, or tree-ring reconstructed flows not subject to diversions that quantify the natural flow of the basin, does not show long-term trends. Therefore, any long-term, ongoing trend in the historical time series of inflow to GSL can be attributed to human water use depletions within the GSL Basin. Mean inflows to GSL were determined for the first and last 30 years of the historical time series in order to establish starting and ending points for determining input reductions. There is some arbitrariness in this selection of 30 years, but it is a common averaging period used for climate averages as it spans a period longer than the typical annual and decadal frequencies present in many hydrologic and climate series. A 30-year moving average was used to determine the general trend of input reductions in the GSL Basin, $Q_{D,Pmean}$, $Q_{D,ra}$, $Q_{D,Q+P}$, for their respective inflow reconstructions. Note that the input reductions associated with the primary inputs hindcast were determined using the same methods as the reductions associated with the reconstructed inflows, with early and late means for start and end points and trends for decreasing primary inputs.

3.10 Natural Water Surface Elevation

The water mass balance in Equation 3 was solved using implicit finite differences to calculate what the lake volume and corresponding WSE would have been given reconstructed natural flows, $Q_{N,Pmean}$ and $Q_{N,ra}$. With an initial WSE of $WSE_{i=0}$ = 1280.267 meters on 1847-10-01 (the beginning of water year 1848), the inflow, precipitation, and evaporation for each water year, i, were used to step ahead to a new lake volume, V_i, and corresponding WSE_i at the end of the water year. Evaluation of the fluctuations in the annual WSE indicate that end of water year WSE_i + 0.15 meters better represents the mean annual WSE over a water year, and therefore this value was used to determine $A_{L,i}$ in the calculation of area dependent precipitation and evaporation volumes. SCF was calculated based on the lake volume of the previous water year. The natural flow and associated WSE were not calculated for the primary inputs hindcast because it has built into it the historical area of the lake (A_L is on the left-hand side of equation 15) and adding estimated depletion to this would not account for the effect of larger lake area associated with the resulting higher lake levels.

3.11 Hindcast Performance, Validation and Error

The metrics used to evaluate and validate hindcast performance and estimate error include the coefficient of variation (*CV*), Root Mean Square Error (*RMSE*), normalized RMSE (*nRMSE*), Nash-Sutcliffe Efficiency (*NSE*), and Kling-Gupta Efficiency (*KGE*). The formulas for each are as follows:

$$CV = \frac{\sigma}{\mu} \tag{19}$$

$$RMSE = \sqrt{\frac{1}{n}\sum_{i=1}^{n}(S_i - O_i)^2} \tag{20}$$

$$nRMSE = \frac{RMSE}{\mu_{obs}} \tag{21}$$

$$NSE = 1 - \frac{\sum_{i=1}^{n}(S_i - O_i)^2}{\sum_{i=1}^{n}(O_i - \bar{O})^2} \tag{22}$$

$$KGE = 1 - \sqrt{(r-1)^2 + \left(\frac{\sigma_{sim}}{\sigma_{obs}} - 1\right)^2 + \left(\frac{\mu_{sim}}{\mu_{obs}} - 1\right)^2} \tag{23}$$

where σ = standard deviation; μ = mean; *S* = the simulated value; *O* = the observed value; and *r* = Pearson correlation coefficient. The *CV* was used to evaluate the performance of the evaporation hindcasts while the *RMSE*, *nRMSE*, *NSE*, and *KGE* were used to evaluate the precipitation and validate inflow hindcasts. In order to determine which hindcast to use in the final inflow reconstruction during certain time periods, all three inflow hindcasts were compared with measured inflow for a validation period, 1950-2023, while the *Pmean* and *ra* hindcasts were comparted with the *PRISM* hindcast for a test period, 1896-1949.

4 Results

4.1 Evaporation

Evaporation depths and volumes over GSL are shown in Figure 4. The mass balance time series of evaporation depth, $E_{L,MB}$, for the years all measured data were available, 1950-2023 (Figure 4a, black solid line), was found to have a mean annual depth of 1.08 m. The mass balance freshwater evaporation depth, $E_{f,MB}$ (Figure 4a, gray solid line), has mean, $E_{f,mean}$, of 1.16 m (Figure 4a, gray dashed line) and standard deviation 0.1 m, reflecting a *CV* of less than 0.1. This small *CV* supports the approximation of E_f as a constant (i.e., $E_f = E_{f,mean} = 1.16$ m) for use in Equation 8 when calculating the hindcast evaporation depth over the lake, E_L (Figure 4a, pink solid line).

4.2 Precipitation

PRISM precipitation depths were used along with measured USGS streamflow in Equation 9 for years both datasets were available, 1950-2023, to estimate the average GSL Basin runoff ratio, $r = 0.13$ (Figure 5a), and in Equation 10 for years 1896-2023 to estimate the basin to lake precipitation ratio, $a = 1.55$ (Figure 5b). The mean annual PRISM precipitation depth over the lake, $P_{L,Pmean}$, is 0.341 m (Figure 6a, gray line). Based on the assumption of constant values for *r*, *a*, and $E_{f,mean}$, a hindcast times series was calculated for precipitation depth over the lake, $P_{L,ra}$ (Figure 6a, purple line), for the years from 1848-2023 using Equation 11, which is driven by WSE that inform lake volume change, lake area, and SCF. The mean depth of $P_{L,ra}$ for the years 1896-2023 is 0.363 m, which is 6.5% more than the mean $P_{L,PRISM}$ (Figure 6a, black line) for the same period. Comparing evaluation metrics for $P_{L,ra}$ and $P_{L,PRISM}$ on the overlapping years, the *RMSE* is 0.122 m, reflecting a normalized *RMSE* of 36%, which is rather high. Interestingly, the *NSE* is -0.33, indicating that $P_{L,Pmean}$ is a better predictor of precipitation depth over the lake than $P_{L,ra}$, while the *KGE* is 0.44, indicating $P_{L,ra}$ is a reasonable predictor of precipitation depth over the lake. Both $P_{L,ra}$ and $P_{L,Pmean}$ were used to estimate hindcasts of inflow to GSL and these metrics for the precipitation should be held in mind when interpreting each inflow hindcast.

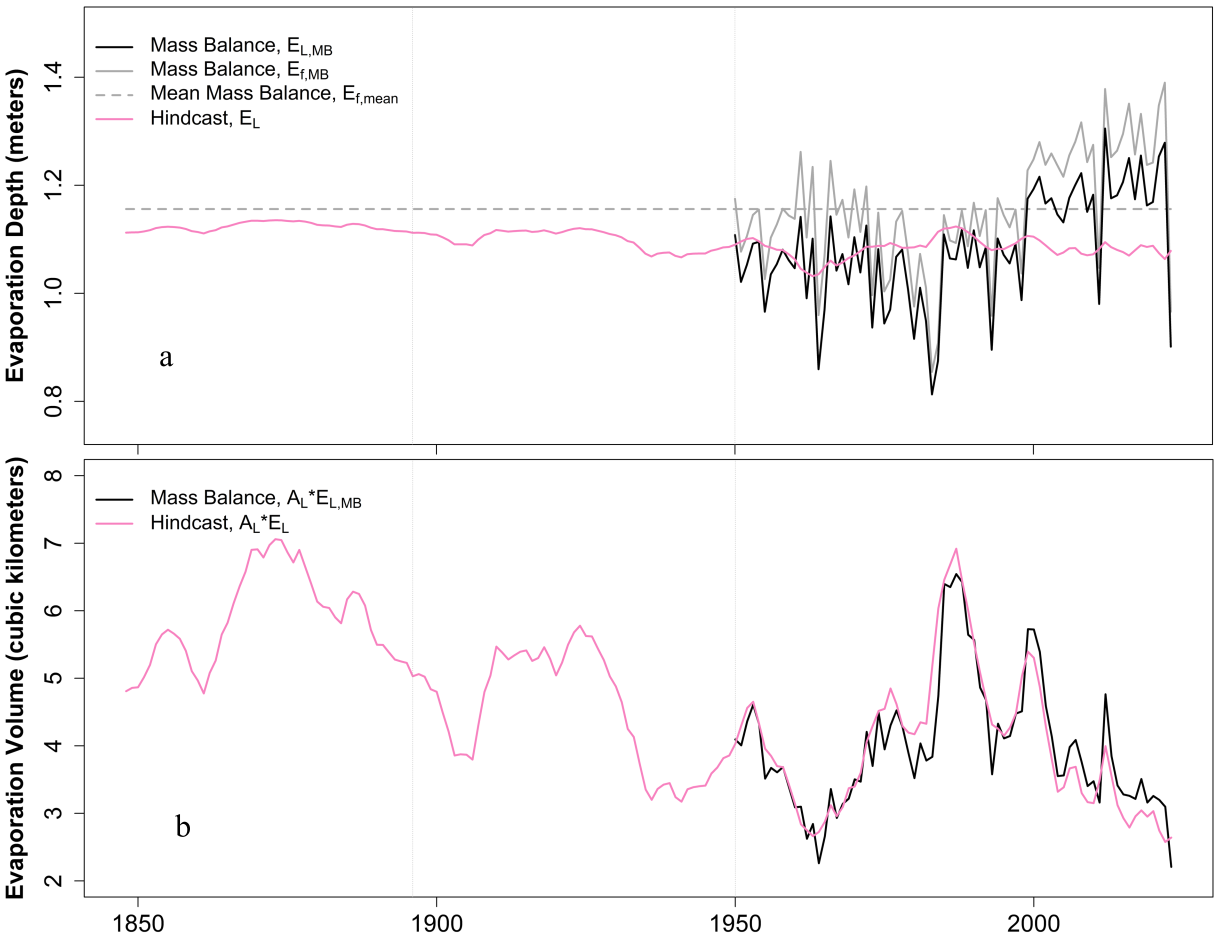

Figure 4. Evaporation (a) depths and (b) volumes over GSL. Results using measured data for mass balance closure over the years 1950-2023 include mass balance freshwater evaporation depth ($E_{f,MB}$, gray solid line), its mean of 1.16 m ($E_{f,mean}$, gray dashed line), and mass balance evaporation depth ($E_{L,MB}$, black solid line). Hindcast results for the years 1848-2023 include evaporation depth over the lake (E_L, pink solid line).

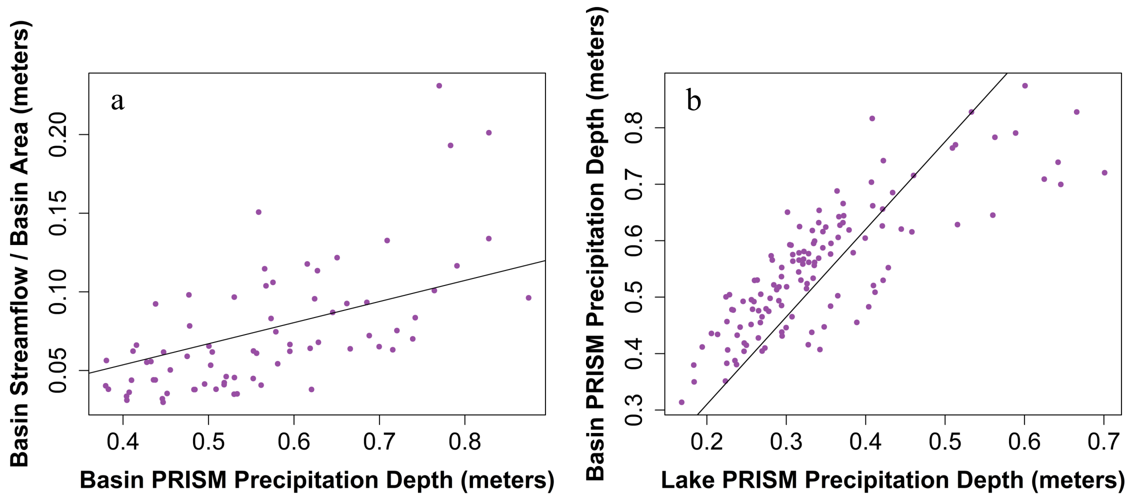

Figure 5. (a) Streamflow volume and precipitation volume in the GSL Basin and the linear relationship between the two (black line) representing the runoff ratio, $r = 0.13$ (Equation 9). (b) Precipitation depth over the GSL Basin and lake and the linear relationship between the two (black line) representing the basin to lake precipitation ratio, $a = 1.55$ (Equation 10).

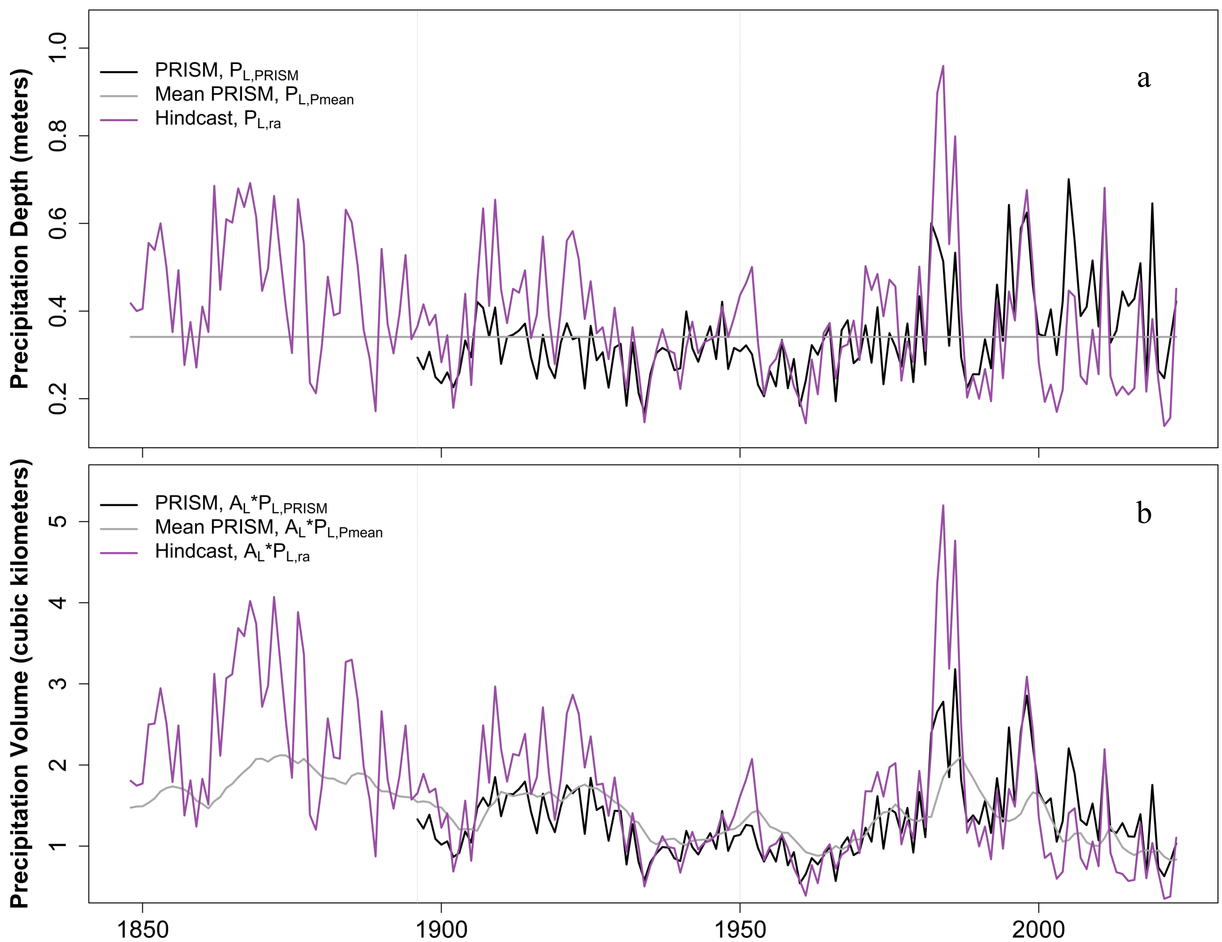

Figure 6. Precipitation depths (a) and volumes (b), including PRISM data over the lake (black solid line), mean PRISM data over the lake (gray solid line), and calculated depth over the lake using constant *r* and *a* (purple solid line).

4.3 Inflow Hindcasts

Inflow hindcast results are shown in Figure 7. All three inflow hindcasts were compared with measured inflow (black line) in a validation period, 1950-2023, and with the *PRISM* hindcast (green line) in a test period, 1896-1949. All evaluation metrics establish the *ra* hindcast (blue line) as a more accurate hindcast than the *Pmean* hindcast (red line) for the validation period, 1950-2023 (Table 1, “Validation” columns), and the *Pmean* hindcast as a more accurate hindcast than the *ra* hindcast for the test period, 1896-1949 (Table 1, “Test” columns). These metrics for the inflow hindcasts should be held in mind when interpreting each inflow reconstruction.

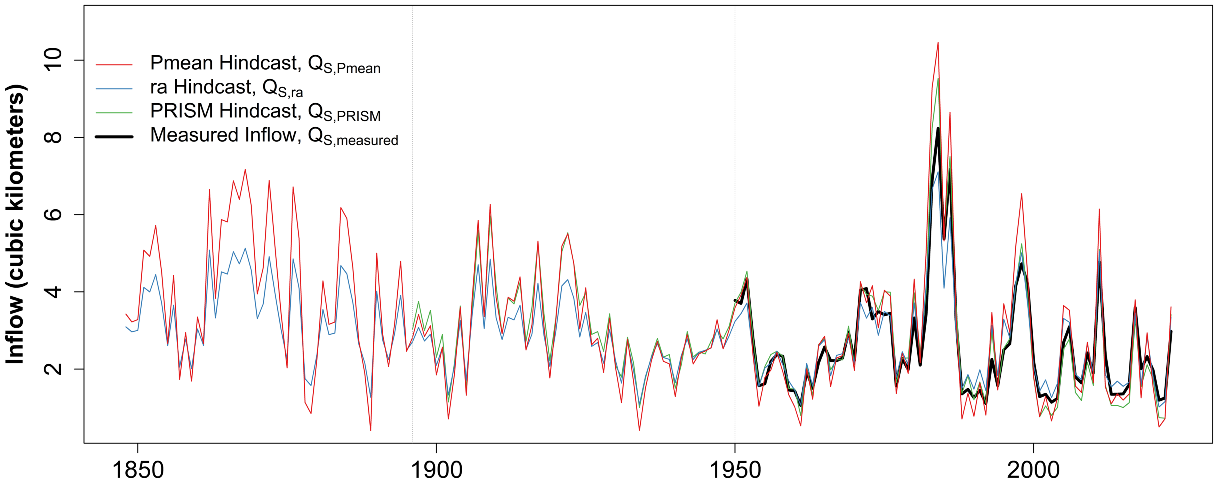

Figure 7. Inflow hindcast results for *Pmean* ($Q_{S,Pmean}$, red line), *ra* ($Q_{S,ra}$, blue line), and *PRISM* ($Q_{S,PRISM}$, green line). Measured inflow (black line) is included for comparison.

Table 1. Evaluation metrics for the inflow hindcasts in Figure 7 for the periods 1896-1949 and 1950-2023.

Evaluation Metric	Test (1896-1949)		Validation (1950-2023)		
	Pmean	*ra*	*Pmean*	*ra*	*PRISM*
NSE	0.93	0.81	0.76	0.92	0.92
KGE	0.86	0.70	0.61	0.86	0.82
RMSE	0.28 m	0.47 m	0.69 m	0.41 m	0.39 m
nRMSE	9%	15%	27%	16%	15%

4.4 Input Reductions Inferred from Reconstructions and Hindcasts

Two reconstructed times series were developed for inflow to GSL, $Q_{R,Pmean}$ and $Q_{R,ra}$ (Equations 16 and 17, respectively) using the respective *Pmean* and *ra* inflow hindcasts for 1848-1895, the PRISM inflow hindcast, $Q_{S,PRISM}$, for 1896-1949, and the measured streamflow, $Q_{S,measured}$, for 1950-2023. The *Pmean* and *ra* reconstructed inflows are shown in Figure 8a, specifying the individual components, *Pmean* hindcast (red solid line), *ra* hindcast (blue solid line), *PRISM* hindcast (green solid line), and measured streamflow (black solid line). Also included are the 30-year moving averages (black solid lines). Note the moving averages are separate for *Pmean* and *ra* for 1848-1895 and then overlap for the remainder of the reconstruction where both use the *PRISM* inflow hindcast and measured streamflow. Also indicated are the starting and ending points of the moving average represented by 30-year spans (horizontal dashed lines).

Similarly, a hindcast of primary inputs to GSL, Q_S+P_L*A_L, was calculated for 1848-2023 using Equation 15. As with the inflow hindcasts, change in lake volume and inflows due to groundwater, mineral extraction, and west desert pumping are known volumes for the entire period and therefore predetermined, and the mean freshwater mass balance evaporation, $E_{\mathrm{f,mean}}$, was also used in Equation 15. The results for the primary inputs hindcast are shown in Figure 8b along with the 30-year moving average (black solid line) as well as the 30-year spans representing the starting and ending points of the moving average (horizontal dashed lines).

The reduced input, representing changes to inflow into GSL between 1848 and 2023, was inferred by taking the difference between the starting and ending points, defined by the 30-year spans (dashed horizontal lines) for each reconstruction method. The decline in the 30-year moving averages seen in *Pmean* and *ra* in Figure 8a and the primary inputs in Figure 8b approximate the input reductions due to water depletions over the historical record. These input reductions were used to determine time series for the *Pmean* and *ra* reconstructions, $Q_{D,Pmean}$ and $Q_{D,ra}$, and the primary inputs hindcast, $Q_{D,Q+P}$. Starting points of $Q_D = 0$ in 1848 were used based on the respective starting point mean flows for *Pmean* (red dashed line, Figure 8a), *ra* (blue dashed line, Figure 8a), and primary inputs flows (brown dashed line, Figure 8b). Ending points in 2023 were used based on the recent mean measured inflow (black dashed lines, Figures 8a and b). The Q_D in all three time series were increased from $Q_D = 0$ in 1848 to their respective recent magnitudes by 1960, $Q_D = Q_{start} - Q_{end}$, based on the rate inferred by the general trend and shape of the 30-year moving averages. The resulting current depletion magnitudes, Q_D, are 2.26 km^3/yr, 1.41 km^3/yr, and 2.60 km^3/yr for *Pmean*, *ra*, and the primary inputs, respectively (Figure 9). Note that the selection of 1960 as the year to switch from increasing consumptive use to flat consumptive use is based on the 30 years means in Figure 8 essentially flattening out by then. While recognizing the uncertainty in selection of this point is about plus or minus 15 years, this uncertainty does not tangibly affect our results.

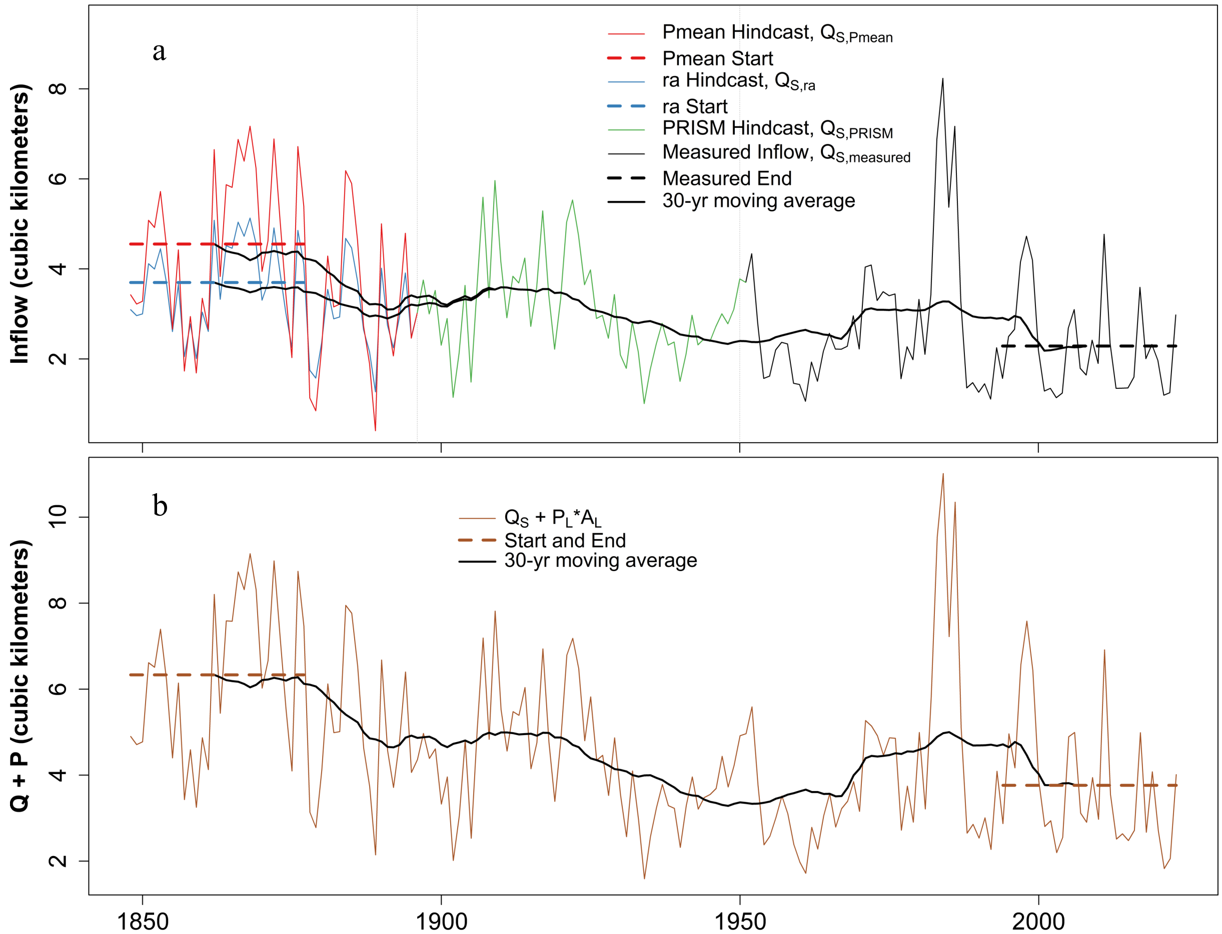

Figure 8. (a) Inflow reconstructions using $Q_{S,Pmean}$ (red line) and $Q_{S,ra}$ (blue line) for 1848-1895, $Q_{S,PRISM}$ (green line) for 1896-1949, and $Q_{S,measured}$ (black line) for 1950-2023. Also included are the 30-year moving averages (black lines) and the 30-year spans representing the start and end of the moving average (dashed lines). (b) Primary inputs hindcast (brown line) with 30-year moving average and 30-year spans representing start and end of the moving average (dashed lines).

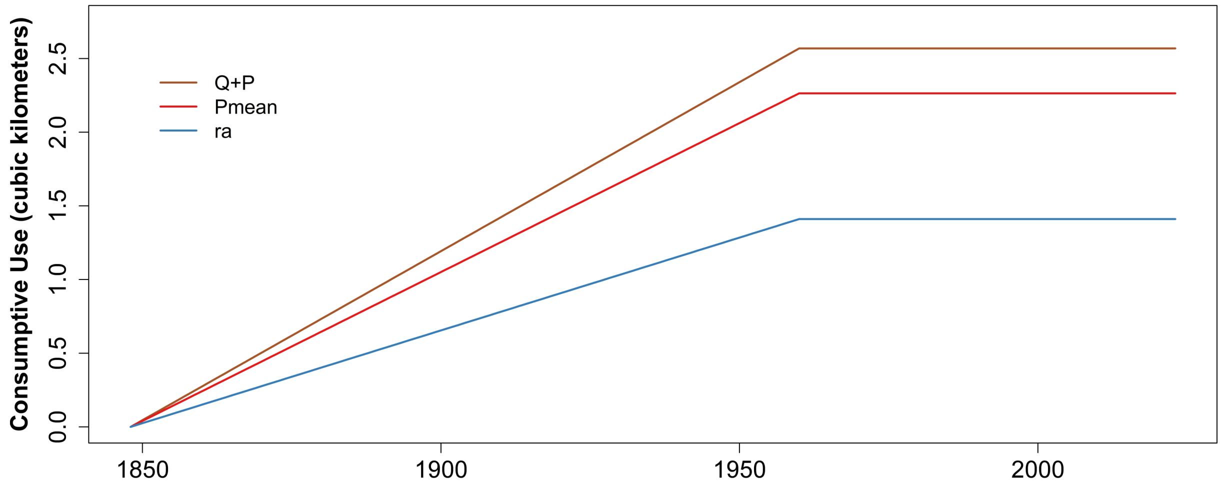

Figure 9. Input reductions inferred from reconstructions and hindcasts are 2.26 km³/yr, 1.41 km³/yr, and 2.60 km³/yr for *Pmean*, *ra*, and the primary inputs, respectively.

4.5 Natural Inflow Reconstructions and Associated Water Surface Elevation

The Q_D from Figure 9 were added to the respective *Pmean* and *ra* reconstructed flows in Figure 8a based on Equation 18 to develop two estimated time series of natural flow into GSL, $Q_{N,Pmean}$ and $Q_{N,ra}$ (Figure 10). By construction, neither the *Pmean* nor *ra* time series for natural flow have a trend. The time series of estimated WSE corresponding to the *Pmean* and *ra* natural flows are presented in Figure 11 and show the current decline in WSE due to reduced inflow to be 4.59 m and 2.82 m, respectively.

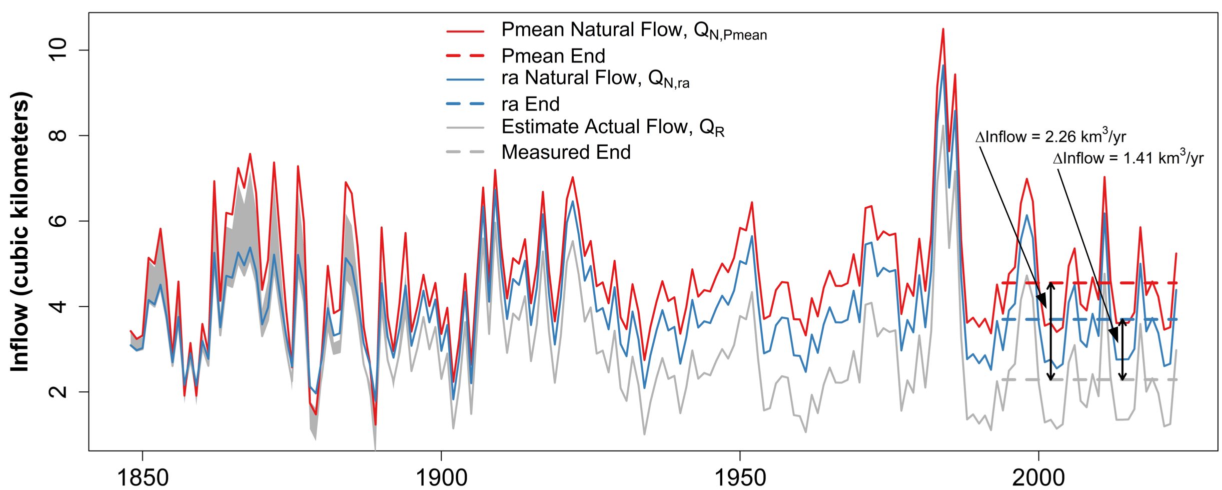

Figure 10. Reconstructed natural inflows to GSL $Q_{N,Pmean}$ (red line) and $Q_{N,ra}$ (blue line), not including depletions, shown in comparison to the respective reconstructed inflows (gray line with shading where they diverge prior to 1896).

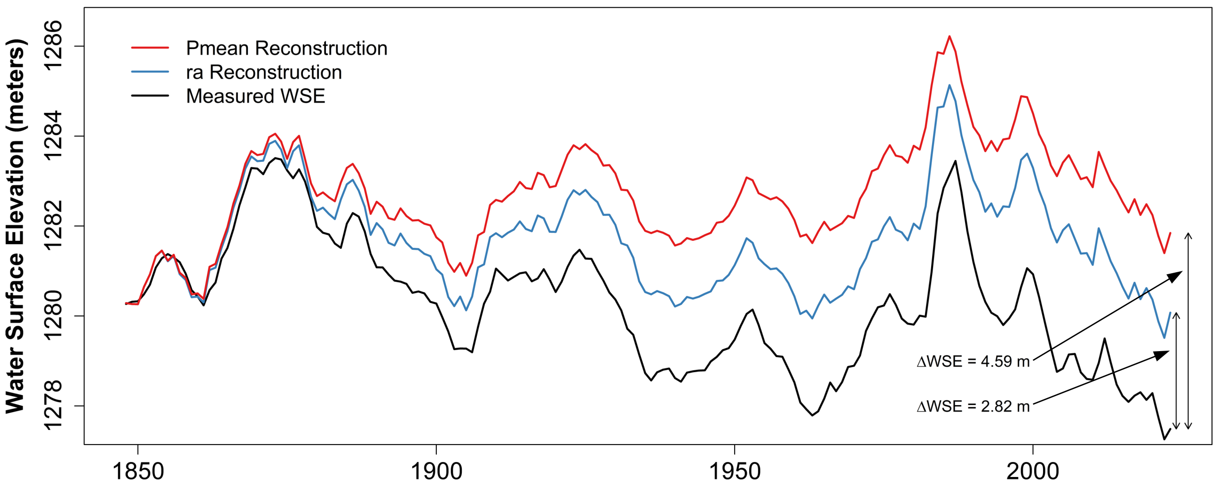

Figure 11. Great Salt Lake water surface elevation based on respective reconstructed natural inflows, $Q_{N,Pmean}$ (red line) and $Q_{N,ra}$ (blue line), shown in comparison to USGS measured water surface elevation (black line).

4 Discussion

The time series of mass balance evaporation depth over GSL, $E_{L,MB}$ (dotted black line, Figure 4a), is generally consistent with the mass balance results reported in Figure 10 of Mohammed and Tarboton (2012), and both time series produce a mean annual evaporation depth of approximately 1.1 m. The time series of mass balance freshwater evaporation depth, $E_{f,MB}$ (solid gray line, Figure 4), calculated using Equation 5 has mean depth, $E_{f,MBmean}$, of 1.16 m, which differs from the mean annual freshwater evaporation depth of 1.29 m that Mohammed and Tarboton calculated using climate data. They point out that GSL WSE modeled using a freshwater evaporation depth of 1.29 m is consistently lower than observed WSE (Figure 11 of their publication), suggesting that 1.29 m may be an overestimate. The calculations in Mohammed and Tarboton are based on data through 2008, including estimated bathymetry and PRISM modeling methods that have both since been refined. In addition, since the publication of their work, there have been refinements to streamflow datasets and the state equation for estimating GSL salinity, which affect measured streamflow and the calculation of SCF and therefore the mass balance. It is for these reasons that we recalculated the value of $E_{f,MBmean}$ for use in our mass balance hindcasts rather than using their published values.

Overall, the metrics comparing the *Pmean*, *ra*, and *PRISM* inflow hindcasts indicate that all hindcast methods give a good prediction of inflow that enables interpretation of how inflows have been reduced over the historical record of WSE measurement and the associated uncertainty (Figure 7, Table 1). In evaluating these, we feel that the *Pmean* hindcast best captures long-term average lake inflow because it has better test period evaluation metrics and is not subject to runoff ratio biases. The differences among the methods serve as an indicator of uncertainty which is small relative to the overall magnitude of the inflow reductions that are interpreted as being due to human consumptive use depletions. The *Pmean* hindcast using constant precipitation underestimates dry periods and overestimates wet periods ($Q_{S,Pmean}$, red solid line, Figure 7) with a relatively high *RMSE* (0.70 m) during the validation period, which is 27% of the mean (*nRMSE*) during that same period. Because of this, we were motivated to develop a hindcast that better represents precipitation and its natural variation to use in the mass balance. Taking advantage of the correlations between basin precipitation, lake precipitation, and lake inflow, the *ra* hindcast precipitation we developed was estimated using a constant basin runoff ratio, *r*, and constant basin to lake precipitation relationship, *a*. The performance metrics are better for the *ra* inflow hindcast ($Q_{S,ra}$, blue line, Figure 7) than the *Pmean* hindcast for the validation period, 1950-2023. It is apparent in Figure 7 that the variability of the *Pmean* hindcast is amplified relative to the *ra* hindcast for the full period (1848-2023). However, the *ra* hindcast is generally below the *Pmean* hindcast prior to 1900. Although the two hindcasts overlap after 1900, crossing nearly every time there is a high-low or low-high transition, the low offset of the *ra* hindcast noticed before 1900 does not appear in later years and also does not appear in comparison to measured streamflow. This early period coincides with the period prior to significant water development and, therefore, significant depletions, when the GSL Basin was just being settled. Since r was calculated using present day precipitation and streamflow, it includes some CU effects. The *r* for the first 50 years or more (e.g., 1848-1900) may be expected to be more than our calculated *r* and we surmise that this may be the cause for the *ra* hindcast being less than the *Pmean* hindcast during that time. Another place this effect can be seen is when comparing the mean precipitation depth for *ra* for the years 1900-2023 and 1848-1900, which are 0.36 and 0.45 m. Using a larger runoff ratio prior to 1900 would result in higher flow than the *ra* hindcast flow, likely closer to the *Pmean* hindcast flows. In addition, when comparing these hindcasts (Figure 8a) with the primary inputs hindcast (Figure 8b) for the early period, 1848-1895, the *Pmean* and primary inputs hindcast are very similar and there is no bias or error included in the primary inputs hindcast due to precipitation. Thus, while the *ra* hindcast is better at capturing one to two year time scale variability, we feel that the *Pmean* hindcast, averaged over a longer period, better captures long-term average lake inflow.

When summing detailed CU to determine overall CU for a basin, like the method used for existing estimates for the GSL Basin, any diversions into or out of the basin would be included in the final result. The transbasin diversions that enter the GSL Basin fulfill CU within the basin but do not contribute to the decrease in flow into the lake or otherwise affect the lake volume. We estimated the decrease in GSL inflow based on changes in volume of the lake and therefore these types of diversions are not included in our result. However, we believe that they are effectively part of the CU reported by Wurtsbaugh et al. (2017) and the GSL Strike Team (GSLST, 2023). Therefore, for comparison to our results it is necessary to remove these diversions from the existing estimates of CU. The average annual transbasin diversion from the Colorado River Basin to the GSL Basin in Utah between 2001 and 2020 was 145,700 AF or 0.18 km^3 (Bureau of Reclamation, 2022). This is similar to the 0.16 km^3/yr transbasin diversion that Wurtsbaugh et al. (2017) reported and included in their water mass balance calculations. Subtracting these transbasin inputs from the reported CU values we are comparing to, we get an equivalent 2.42 km^3/yr for GSL Strike Team and 1.54 km^3/yr for Wurtsbaugh et al. (2017). This is similar to the range of our results, 1.41-2.26 km^3/yr, based on the range of *ra* and *Pmean*. However, as noted above, our *ra* hindcast appears to be biased low in early years due to *r* having been calculated with streamflow that includes CU and applying it to a time when there presumably were nearly no depletions. Therefore, the estimate of 2.26 km^3/yr from the *Pmean* hindcast is more defensible and is very close to the GSL Strike Team results, yet it is approximately 50% higher than the results from Wurtsbaugh et al. (2017). This leads us to believe that Wurtsbaugh et al. (2017) may not have had as complete information or data as was available for this study and that was used by the GSL Strike Team. On the other hand, the GSL Strike Team included CU from areas of the basin that are hydrologically disconnected from the lake, like the west desert, which does not affect the GSL WSE and makes an estimate based on summing CU higher. It is also worth noting that the characteristics of the early trend in both the *Pmean* and *ra* flow hindcasts mimic what Wurstbaugh et al. (2017) asserted about the majority of CU occurring shortly after the GSL Basin was settled, and the characteristics of the recent trend mimic the constant CU shown in the estimate by the GSL Strike Team.

5 Conclusion

Reductions in streamflow into the GSL are responsible for declines in the terminal lake's WSE. Present estimates of consumptive water use within the GSL Basin based on summing detailed uses and return flows are disparate and range from 1.5 to 2.4 km^3/yr. This paper offers an additional line of evidence for quantifying consumptive use by estimating inflow depletions through volume reconstruction from records of WSE. We analyzed annual changes in lake volume for GSL to reconstruct inflow corresponding to the full historical record of WSE and estimated the magnitude of CU in the basin and associated lake level decline for the water years 1848-2023. Our analysis included developing hindcasts for annual evaporation and precipitation depths over the lake and inflow volume to the lake, from which we reconstructed annual streamflow using a water mass balance. Two methods were used to estimate precipitation, giving us a range for CU of 1.41-2.26 km^3/yr and the associated lake level decline of 2.82-4.59 m. Our hindcast of evaporation depth over the lake is consistent with previous mass balance estimates for the years 1950-2010 but was extended to include the entire 1848-2023 period. A bias may be present in the *ra* hindcast of precipitation using a constant runoff ratio due to its dependency on measured streamflow that includes CU. This bias would be more pronounced, and would therefore result in an underestimate of CU, during years immediately after the initiation of irrigated agriculture following Mormon Pioneer settlement in the GSL Basin starting in 1847. Because of this bias in the *ra* based estimate, we believe that the *Pmean* estimate of CU in GSL Basin of 2.26 km^3/yr based on constant average precipitation is better and lake level decline due to this estimate is closer to 4.59 meters. These findings are important because they quantify the degree to which CU has impacted the lake and serve as a reference for efforts towards conservation and other water management actions aimed at restoring the lake to levels where it better supports its uses.

Acknowledgments

This research was funded by the Utah Water Research Laboratory and the Sant Foundation Endowed Professorship to David Tarboton. The authors are grateful for this support.

Open Research

All scripts and data used in this paper have been published in HydroShare (Tarboton, 2023a,c; Tarboton and Merck, 2023; Merck and Tarboton, 2023) and added to the publicly available HydroShare Collection of Great Salt Lake Data (Tarboton, 2023b).

References

Aldrich, T.W., Paul, D.S. (2002), Avian ecology of Great Salt Lake. Great Salt Lake: An overview of change (J.W. Gwynn, ed). *Special publication of the Utah Dept. of Natural Resources.*

Barnes, B.D., & Wurtsbaugh, W.A. (2015), The effects of salinity on plankton and benthic communities in the Great Salt Lake, Utah, USA: a microcosm experiment. *Canadian Journal of fisheries and Aquatic Sciences, 72*(6):807–17.

Bekker, M. F., DeRose, R. J., Buckley, B. M., Kjelgren, R. K., & Gill, N. S.(2014), A 576-Year Weber River Streamflow Reconstruction from Tree Rings for Water Resource Risk Assessment in the Wasatch Front, Utah. *Journal of the American Water Resources Association, 50*(5),1338-1348. doi:10.1111/jawr.12191

Bureau of Reclamation, https://qcnr.usu.edu/coloradoriver/files/news/Tranbasin-Fact-Sheet.pdf

Daly, C., Halbleib, M., Smith, J. I., Gibson, W. P., Doggett, M. K., Taylor, G. H., Curtis, J. & Pasteris, P. P. (2008), Physiographically sensitive mapping of climatological temperature and precipitation across the conterminous United States. *International Journal of Climatology, 28*(15): 2031-2064, http://dx.doi.org/10.1002/joc.1688

DeRose, R. J. et al. A millennium-length reconstruction of Bear River stream flow, Utah. J. Hydrol. 529, 524–534 (2015).

GSL Strike Team. (2023). *Great Salt Lake Policy Assessment A synthesized resource document for the 2023 General Legislative Session.* Retrieve from https://gardner.utah.edu/wp-content/uploads/GSL-Assessment-Feb2023.pdf?x71849

Hahl, D.C. Dissolved-Mineral Inflow to Great Salt Lake and Chemical Characteristics of the Salt Lake Brine: Summary for Water Years 1960, 1961, and 1964; Water-Resources Bulletin 10; Utah Geological Survey: Salt Lake City, UT, USA, 1968; 35p.

Hahnenberger, M. & Nicoll, K. (2012), Meteorological characteristics of dust storm events in the eastern Great Basin of Utah, U.S.A. *Atmospheric Environment, 60*:601-612. doi:10.1016/j.atmosenv.2012.06.029

Hahnenberger, M. & Nicoll, K. (2014), Geomorphic and land cover identification of dust sources in the eastern Great Basin of Utah, U.S.A. *Geomorphology, 204*:657-672. doi:10.1016/j.geomorph.2013.09.013

IWJV, Intermountain West Joint Venture. 2016. Retrieved from www.iwjv.org

Lall, U. & Mann, M. (1995), "The Great Salt Lake: A barometer of low-frequency climatic variability," Water Resources Research, 31(10): 2503-2515, https://doi.org/10.1029/95WR01950.

Lang, O. I., Mallia, D., & McKenzie Skiles, S. (2023). The shrinking Great Salt Lake contributes to record high dust-on-snow deposition in the Wasatch Mountains during the 2022 snowmelt season. *Environmental Research Letters, 18*(6): 064045, http://doi.org/10.1088/1748-9326/acd409.

Loving, B.L., Waddell, K.M. & Miller, C.W. (2000), Water and Salt Balance of Great Salt Lake, Utah, and Simulation of Water and Salt Movement through the Causeway, 1987–98; U.S. Geological Survey: Salt Lake City, UT, USA, 2000. Retrieved from https://pubs.usgs.gov/wri/2000/4221/report.pdf

Merck, M. F. and D. G. Tarboton, (2023), The Salinity of the Great Salt Lake and Its Deep Brine Layer. *Water, 15*(8), doi:10.3390/w15081488

Merck, M.F. and Tarboton D.G. (2023). Reconstructing inflows to the Great Salt Lake from historical lake level records, HydroShare, http://www.hydroshare.org/resource/65ac72dd2ce8474983e21a5396159f7b

Mohammed, I.N. & Tarboton, D.G. (2012), An examination of the sensitivity of the Great Salt Lake to changes in inputs. *Water Resources Research*. 48, W11511. doi:10.1029/2012WR011908

Penrod, E (2023), 'If the Great Salt Lake went away, the world would be poorer for it': How Utah's terminal lake helps feed the world. *The Salt Lake Tribune.* https://www.sltrib.com/news/environment/2023/12/08/if-great-salt-lake-went-away-world/

Stephens, D.W. (1990). Changes in lake levels, salinity and the biological community of Great Salt Lake (Utah, USA), 1847-1987. *Hydrobiologia*, 197: 139-146.

Tarboton, D, and M Merck. (2023). Great Salt Lake Bathymetry. HydroShare. http://www.hydroshare.org/resource/582060f00f6b443bb26e896426d9f62a.

Tarboton, D. (2023a). Streamflow entering the Great Salt Lake. HydroShare. http://www.hydroshare.org/resource/bb2bba84e1d5424db9211a991a7e5dd8

Tarboton, D. (2023b). Collection of Great Salt Lake Data. HydroShare. http://www.hydroshare.org/resource/b6c4fcad40c64c4cb4dd7d4a25d0db6e

Tarboton, D. (2023c). Great Salt Lake Level and Volume Time Series, HydroShare, http://www.hydroshare.org/resource/45b43d72928048a8bc10a009d932f769

Tikalsky, B. P. (2007). *An 828 year streamflow reconstruction for the jordan river drainage basin of northern Utah* (master's thesis). Retrieved from ScholarsArchive. (https://scholarsarchive.byu.edu/etd/1444/). Provo, Utah: Brigham Young University.

UGS Survey Notes. (2021). *Glad you asked: does Utah really use more water than any other state?* Retrieved from https://ugspub.nr.utah.gov/publications/survey_notes/snt50-2.pdf

USCB. (2023). *United States Census Bureau QuickFacts*. Retrieve from https://www.census.gov/quickfacts/geo/chart/UT,US/PST120222

Waddell, K.M. & Fields, F.K. (1977) Model for evaluating the effects of dikes on the water and salt balance of Great Salt Lake, Utah: Utah Geological Survey Water-Resources Bulletin 21, 54 p.

WHSRN, Western Hemisphere Shorebird Reserve Network (2016). http://www.whsrn.org Accessed 3/2016

Wurtsbaugh, W. A., Miller, C., Null, S. E., Wilcock, P., & Hahnenberger, M. (2016), *Impacts of Water Development on Great Salt Lake and the Wasatch Front*. Logan, Utah: Utah State University.

Wurtsbaugh, W. A., Miller, C., Null, S. E., DeRose, R. J., Wilcock, P., Hahnenberger, M., Howe, F., & Moore, J. (2017), Decline of the world's saline lakes. *Nature Geoscience*. doi: 10.1038/ngeo3052.